Acta Materialia 242 (2023) 118466

Contents lists available at ScienceDirect

Acta Materialia

journal homepage: www.elsevier.com/locate/actamat

Full length article

Unusual precipitation induced by solute segregation in coherent twin boundary in titanium alloys

Chaoqiang Liu[a], Xin Hu[a], Lin Qi[b], Houwen Chen[b,c], Zhiqiao Li[b], Xiaoyong Zhang[a], Hongge Yan[d], Kechao Zhou[a], Min Song[a,*], Yunzhi Wang[e], Jian-Feng Nie[f,*]

[a] State Key Laboratory of Powder Metallurgy, Central South University, Changsha 410083, China
[b] College of Materials Science and Engineering, Chongqing University, Chongqing 400044, China
[c] Electron Microscopy Center, Chongqing University, Chongqing 400044, China
[d] School of Materials Science and Engineering, Hunan University, Changsha 410082, China
[e] Department of Materials Science and Engineering, The Ohio State University, 2041N. College Rd., Columbus, OH 43210, USA
[f] Department of Materials Science and Engineering, Monash University, Victoria 3800, Australia

ARTICLE INFO

Article history:
Received 29 August 2022
Revised 13 October 2022
Accepted 20 October 2022
Available online 21 October 2022

Keywords:
Titanium alloys
Solute segregation
Precipitation
Twin boundary

ABSTRACT

Heterogeneous precipitation and hence the distribution of α and β phase in $\alpha+\beta$ titanium alloys can impact strongly on alloy mechanical properties. The β phase is commonly observed to precipitate heterogeneously at boundaries between α' martensite plates and dislocations inside the martensite, especially in the additively manufactured $\alpha+\beta$ titanium alloys, with a Burgers orientation relationship with the surrounding matrix phase. Here, we report an interesting phenomenon in a Ti-4wt%Mo alloy where the β phase precipitates heterogeneously on Mo-segregated $\{10\bar{1}1\}$ fully coherent twin boundaries (CTBs) within α' martensite, with an unusual Potter orientation relationship with α'. We find that the CTB has a structure resembling that of the β phase and that Mo segregation in the CTB leads to an unusual out-of-plane shift of the segregated atomic columns that makes the local structure almost identical to the β structure, hence serving as a template for β precipitation with the unique orientation relationship. Our findings reveal a novel mechanism via which the distribution of β precipitates can be manipulated effectively for better mechanical properties and could be extended to a group of Ti alloys including the current workhorse alloy Ti-6Al-4V and more broadly to other engineering alloys.

1. Introduction

Titanium and its alloys have received considerable attention in the past few decades due to their widespread applications in aerospace, chemical and marine industries [1–3]. Most titanium alloys used in the aerospace industry are comprised of α and β phases, known as $\alpha+\beta$ titanium alloys. These alloys usually have poor comprehensive mechanical properties in as-quenched condition due to the formation of martensite during quenching. Desirable mechanical properties are usually achieved through the decomposition of martensite in subsequent heat treatment processes [4,5]. The products of martensite decomposition are α and β phases. By adjusting the morphology, spatial distribution and volume fraction of the two phases, the $\alpha+\beta$ alloys offer a range of combinations of strength, toughness, and high temperature performance [6–13]. In order to precisely control the formation of α and β phases in the $\alpha+\beta$ titanium alloys and thus tailor the mechanical properties of the alloys, it is essential to understand the phase transformation mechanisms from the martensite to α and β phases.

α' (hexagonal, space group $P6_3/mmc$, $a=0.293$ nm, $c=0.467$ nm [14]) is one of the most common martensite in the quenched $\alpha+\beta$ titanium alloys and it has a lenticular or plate shape and contains a high density of crystallographic defects such as twin boundaries, stacking faults and dislocations [3,15]. The formation of β (body-centered cubic, space group $Im\bar{3}m$, $a=0.331$ nm [26]) during α' martensite decomposition has been studied since the 1970s [16] and is receiving increasing attention in the past 5–10 years due to the rapid development of additively manufactured $\alpha+\beta$ titanium alloys [4,17–25]. The as-built alloys are usually comprised of α' martensite and have relatively poor mechanical properties, and many attempts have been made to investigate the relationship between α' martensite decomposition and mechanical properties [4,17–22]. However, studies on the mechanisms of the martensite decomposition and β formation mechanism are relatively less, especially at the atomic scale, even though the atomistic understand-

* Corresponding authors.
E-mail addresses: msong@csu.edu.cn (M. Song), jianfeng.nie@monash.edu (J.-F. Nie).

https://doi.org/10.1016/j.actamat.2022.118466
1359-6454/

ing of the β formation mechanism is critical to further improvement in the distribution of β and hence mechanical properties.

The previous studies [4,19–25] revealed that the spatial distribution and morphology of β phases formed during α' martensite decomposition vary with the ageing temperature and time. The orientation relationship (OR) between the β phase and α' martensite is such that Burgers orientation OR, i.e., $[\bar{1}11]_\beta$ // $[1\bar{2}10]_{\alpha'}$ and $(101)_\beta$ // $(0001)_{\alpha'}$ [16], which is also widely accepted to exist between β and α in all titanium alloys [2,3,7]. Note that α' has almost the same lattice structure and lattice parameters as α (hexagonal, space group $P6_3/mmc$, $a = 0.295$ nm, $c = 0.468$ nm) [14,26]. α' can be actually regarded as the supersaturated α, and the decomposition of α' into α and β can be considered as precipitation of β from the supersaturated α matrix. A recent study [27,28] reported that the formation of β phase inside α' or α matrix is mediated by an intermediate structure. In contrast to the intra-granular precipitation of β, the inter-granular precipitation, e.g., precipitation at twin boundaries, is more representative of heterogeneous phase transformations that is vital to the distribution of precipitates and then the mechanical properties of the metallic alloys. Such as the heterogeneous precipitation of precipitates on dense twin boundaries lead to the change of the morphology and distribution of precipitates, resulting in a noticeable improvement in mechanical properties in magnesium alloys [29]. An exciting paper [30] reported the possibility of forming a massive amount of nanotwins and hence twin boundaries in hexagonal Ti. Therefore, if the β phase could heterogeneously precipitate on the twin boundaries in the α' martensite, its distribution would be dramatically changed by introducing dense nanotwins. However, the β has only been observed to heterogeneously precipitate on the interfaces between martensite plates and at dislocations inside martensite [2,16,21]. Whether its heterogeneous precipitation occurs on twin boundaries and the underlying mechanism remain unclear.

In this paper, we use atomic-resolution high-angle annular dark-field scanning transmission electron microscopy (HAADF-STEM) and first-principles calculations to study this issue in a model titanium alloy containing 4 wt% molybdenum (Mo) (Mo is a typical β stabilizing element). We find that the β phase precipitates heterogeneously on Mo-segregated $\{10\bar{1}1\}$ fully coherent twin boundaries (CTBs) within α' martensite, with an unusual Potter OR with α'. We also find that the CTB has a structure resembling that of the β phase and that Mo segregation in the CTB leads to an unusual out-of-plane shift of the segregated atomic columns that makes the local structure almost identical to the β structure. Hence, the solute segregated CTB serve as a template for β precipitation with the unique OR.

2. Experimental procedures and computation method

Alloy with a nominal composition of Ti-4wt%Mo (wt% is used in the whole paper) was prepared from high-purity Ti and Mo metals by vacuum induction melting. Small samples cut from the ingot were heated to 900 °C (β phase region) and kept for 1 h to acquire the complete β phase, and then water quenched to room temperature to induce martensitic phase transformation and acquire α' martensite. After that, the samples were aged at 400 °C for 4 h, 550 °C for 8 h, or 550 °C for 48 h. All specimens for HAADF-STEM observations were prepared by mechanical polishing to 60–80 μm and then twin-jet electropolishing at −25 °C. The twin-jet solution is comprised of 60% methanol, 35% butanol, and 5% perchloric acid. HAADF-STEM and energy-dispersive X-ray spectroscopy (EDXS) characterizations were carried out in a Cs-corrected FEI Titan G^2 60–300 ChemiSTEM and Spectra 300 (C-FEG) operated at 300 kV and equipped with four windowless silicon-drift X-ray detectors. A 15 mrad convergence semi-angle and an inner-collection semi-angle of 57 mrad were used for HAADF imaging. The atomic-resolution HAADF-STEM images were processed via masking the diffraction spots in its FFT patterns and then inversely transforming using Gatan Digital Micrograph software package. In addition, a geometric phase analysis (GPA) plug-in package running in the Gatan Digital Micrograph was used to show the strain map around misfit dislocation.

To rationalize the segregation of solute atoms and understand the origin of preferential precipitation of β phase at $\{10\bar{1}1\}$ CTB, first-principles calculations were employed, which is based on density functional theory (DFT) and performed within the Vienna *Ab Initio* Simulation Package (VASP) code [31] and uses the Generalized-Gradient Approximation exchange-correlation functional of Perdew-Burke-Ernzerhof [32]. Atoms were treated using projector augmented-wave (PAW) pseudopotentials [33,34]. The cut-off energy was set at 380 eV. The convergence accuracy for the electronic self-consistency was fixed at 10^{-5} eV per cell and the optimization of the atomic geometry was performed until the residual forces were less than 10^{-2} eV/Å. The k-point grid was constructed using the Monkhorst-Pack scheme [35].

Regarding the calculations of segregation energies of solute atoms in $(10\bar{1}1)$ CTB, a supercell containing two $(10\bar{1}1)$ CTBs with a separation distance of 11 $(10\bar{1}1)$ planes was constructed, Fig. 9a. The supercell was relaxed using the *k*-point meshes of 9 × 34 × 2. The supercell lattice parameter normal to the CTB was set to be free to vary, while the other two lattice parameters parallel to the CTB were fixed to a multiple of bulk HCP Ti lattice constants to avoid the effect of high number density CTBs that is artificially introduced in the supercell. The segregation energies (E_{seg}) of different solute atoms occupying the compression or extension site were calculated using the following equation:

$$E_{seg} = \{[E_{twin}(Ti_{N-m}X_m) - E_{twin}(Ti_N)] - m[E_{bulk}(Ti_{M-1}X) - E_{bulk}(Ti_M)]\}/m, \quad (1)$$

where $E_{twin}(Ti_{N-m}X_m)$ and $E_{twin}(Ti_N)$ are the total energies of supercells with and without segregated solute atoms in the CTB, respectively, $E_{bulk}(Ti_{M-1}X)$ and $E_{bulk}(Ti_M)$ are the total energies of matrix supercell with and without dissolved solute atoms, respectively, N and M are the numbers of atoms of the supercell containing two CTBs and the α' matrix supercell, respectively, m is the number of solute atom.

To determine the preferential position of the β structural unit, elastic strain energies caused by the β structural unit at different positions were initially calculated using the supercell in Fig. 11a. The *k*-point meshes was set to be 4 × 34 × 2 for the geometrical relaxation. When the β structural unit was put into the supercell, all atoms in the β structural unit were fixed during relaxation. The elastic strain energies caused by the β structural unit was given by:

$$E_e = E_{final} - E_{initial}, \quad (2)$$

where $E_{initial}$ and E_{final} are the total energies of the supercells before and after the β structural unit forms. To obtain the preferential formation position of the β structural unit, the difference of elastic strain energies (ΔE) caused by the β structural unit at different positions was calculated according to the following equation:

$$\Delta E = E_{e-x} - E_{e-0}, \quad (3)$$

where $E_{e\text{-}x}$ and $E_{e\text{-}0}$ are the elastic strain energies caused by the β structural unit formed at positions near the $(10\bar{1}1)$ CTB and matrix (reference state), respectively. In this study, x could be 1 to 7 in Fig. 11a. To determine the position of the β structural unit in the reference state, the elastic strain energies caused by the β structural unit at different distances from the CTB were calculated, and when the elastic strain energy hardly changes with the increase in distance from the CTB, the corresponding position was defined to

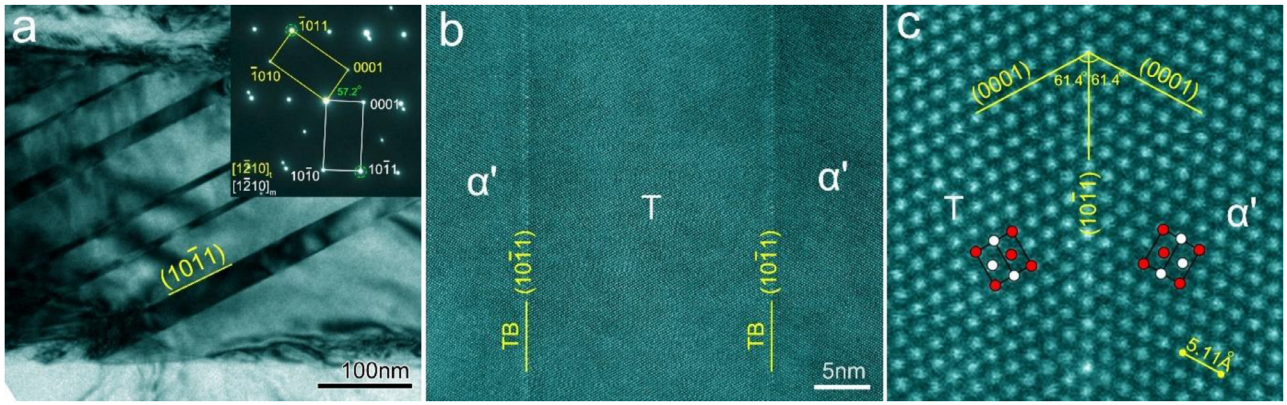

Fig. 1. (a) Bright-field image showing $(10\bar{1}1)$ transformation twins within α' martensite in an as-quenched sample. Inset is the corresponding selected area electron diffraction (SAED) pattern. (b) Low-magnification and (c) atomic-resolution HAADF-STEM images showing $(10\bar{1}1)$ CTBs in the as-quenched sample. Letter T represents transformation twin in α' martensite. Electron beam is parallel to $[1\bar{2}10]_{\alpha'}$ zone axis.

be the position of the β structural unit formed in reference state, marked by number 0 in Fig. 9a.

3. Results

3.1. Characterizations of Mo segregation and β precipitation

Fig. 1a shows a bright-field (BF) image of an internally twinned α' martensite plate viewed along the $[1\bar{2}10]_{\alpha'}$ zone axis in an as-quenched Ti-4Mo alloy. Many $(10\bar{1}1)$ transformation twins with a width of 5–30 nm are visible within the martensite plate. This is similar to those observed in some as-quenched or as-additive-manufactured $\alpha+\beta$ titanium alloys [17,36,37]. Fig. 1b shows a low-magnification HAADF-STEM image of a $(10\bar{1}1)$ twin within the martensite plate. Its width is ~20 nm, and its two CTBs are very straight and strictly parallel to each other, which is different from deformation twins that usually have a lenticular shape and contain many steps on the otherwise fully coherent TBs [38,39]. According to the atomic-resolution HAADF-STEM image of one of the CTBs, Fig. 1c, the CTB has a similar brightness as the twin and the martensite, indicating the apparent absence of Mo segregation in the CTB in the as-quenched condition, since the brightness of a HAADF-STEM image is approximately proportional to the square of atomic number and Mo (42) has a much higher atomic number than Ti (22).

Fig. 2a shows a low-magnification HAADF-STEM image of a $(10\bar{1}1)$ twin in a sample at a very early stage of ageing. Obviously, the two CTBs have a much higher brightness than the α' martensite, suggesting that Mo segregation has occurred in these two CTBs. The Mo segregation is further supported by the EDXS analysis, Fig. 2b. Fig. 2c shows an atomic-resolution HAADF-STEM image of one of the two CTBs. The Mo-rich columns are distributed periodically in the CTB. Fig. 2d shows a hard-sphere model of a $(10\bar{1}1)$ CTB. Extension and compression sites are distributed alternately in the CTB. Careful comparison of atomic arrangements surrounding the Mo-rich columns, Fig. 2c, and those surrounding the compression and extension sites, Fig. 2d, reveals that the Mo atoms segregate to the compression sites.

Fig. 3a shows a low-magnification HAADF-STEM image of a $(10\bar{1}1)$ twin in a sample at a subsequent stage of ageing. Many precipitates are detected on $(10\bar{1}1)$ CTBs. They have an elliptical shape with their major axis parallel to the CTB. Fig. 3b shows the atomic resolution HAADF-STEM image of a small precipitate. According to its corresponding fast-Fourier transform (FFT) pattern, Fig. 3c, the precipitate is determined to be β phase. This is unexpected as the heterogeneous precipitation of β phase was traditionally considered to occur on interfaces between martensite plates or on dislocations inside the martensite plates [2,16]. Careful analysis of the FFT reveals that the OR between the β precipitate and the α' martensite and its transformation twin is such that $(01\bar{1})_\beta$ // $(10\bar{1}1)_{\alpha'/T}$ and $[\bar{1}11]_\beta$ // $[1\bar{2}10]_{\alpha'/T}$, also known as the Potter OR, which is clearly different from the traditionally reported Burgers OR that is in the form of $\{101\}_\beta$ // $\{0001\}_{\alpha'}$ and $\langle\bar{1}11\rangle_\beta$ // $\langle 2\bar{1}\bar{1}0\rangle_{\alpha'}$ [3,16,37]. The stereographic projection of the Potter OR, shown in Fig. 4, indicates that the angle between the $\{101\}_\beta$ and $(0001)_{\alpha'/T}$ in this OR is ~1.4°. In addition, the β phase have a higher brightness than the martensite, implying that they have a higher Mo concentration. The Mo concentration in the β phase was measured to be approximately 19.5 ± 2.5 at.%, based on the quantitative EDXS analyses of 10 particles. This is reasonable since Mo is a typical β stabilizing element and it has a strong tendency to partition to the β phase. Above and under the precipitate in Fig. 3b, $(10\bar{1}1)$ CTBs are still detectable, but Mo segregation has disappeared. This is expected since the formation of the β precipitate would attract Mo atoms, resulting in a Mo-depletion region surrounding the precipitate. Connecting the $(10\bar{1}1)$ CTBs above and under this precipitate, there is a straight line, as indicated by the purple dashed line in the middle of the precipitate, which proves that the β precipitate forms exactly on the coherent region of the $(10\bar{1}1)$ twin boundary, i.e., $(10\bar{1}1)$ CTB.

Fig. 3d shows an enlarged HAADF-STEM image of the top trigeminal boundary of the β phase, α' martensite and its transformation twin, as marked by yellow dashed frame 1 in Fig. 3b. Yellow dashed lines represent the boundaries between the β phase and the α'/twin. Across the boundaries, the β phase and α'/twin is coherent and the misfit between the $(01\bar{1})_\beta$ and $(10\bar{1}1)_{T/\alpha'}$ planes is measured to be about 2.5%, assuming that $a = 0.293$ nm for the α' martensite [26]. The $(10\bar{1}1)$ CTB is parallel to $(01\bar{1})_\beta$, and the atomic arrangement in the CTB and the $(01\bar{1})_\beta$ plane is atomically flat. At both sides of the CTB, atoms in the $(10\bar{1}1)_{\alpha'}$ planes have a wave-like arrangement, as shown by the red and white dots at the left and right sides of the CTB. Careful inspection indicates that three atomic columns near the CTB, marked by red arrows in Fig. 3d, are displaced slightly from their original positions in the $(10\bar{1}1)_{\alpha'}$ planes to the corresponding positions in the $(01\bar{1})_\beta$ plane. Fig. 3e shows an enlarged HAADF-STEM image of the interphase boundary between the β phase and the transformation twin, as marked by the yellow dashed frame 2 in Fig. 3b. This interface is also coherent and the lattice misfit between the $(101)_\beta$ and $(0001)_T$ planes is measured to be ~1.6%. Careful measurements indicate that the $(101)_\beta$ plane is 1.4° away from the $(0001)_T$ plane, which is consistent with the Potter OR, Fig. 4. Fig. 3f shows an enlarged HAADF-STEM image of the interphase boundary between

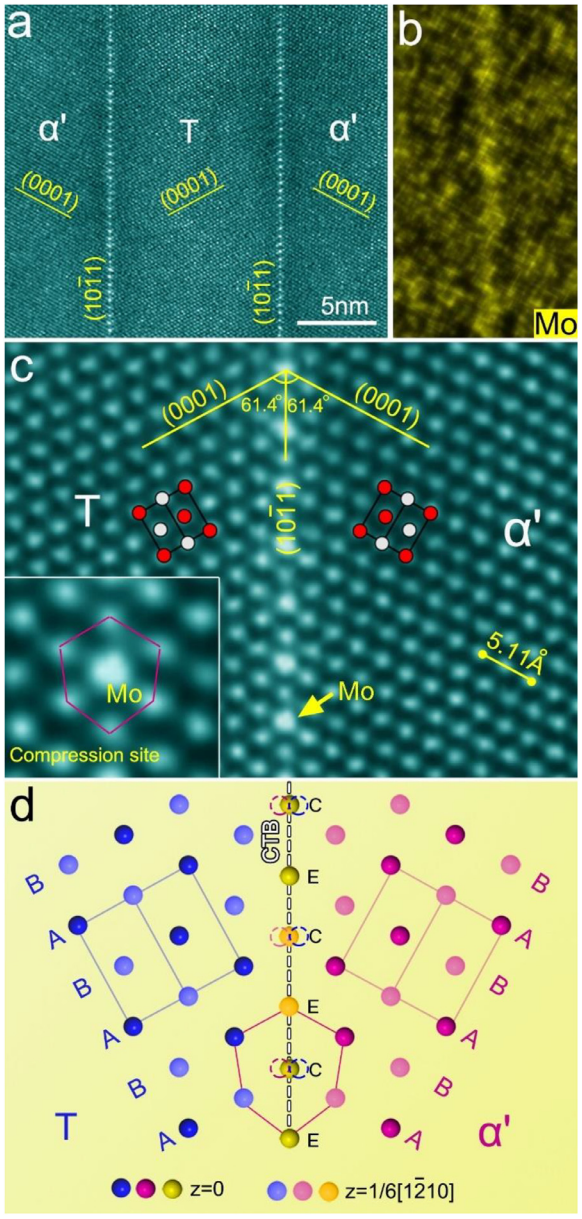

Fig. 2. (a) Low-magnification HAADF-STEM images showing (10$\bar{1}$1) CTBs in a sample aged at 400 °C for 4 h. (b) EDXS-STEM map of the right (10$\bar{1}$1) CTB in (a) showing higher Mo concentration at the CTB. (c) Atomic-resolution HAADF-STEM image showing the periodic distribution of Mo-rich columns in the CTB. Inset in (c) shows the enlarged image around the Mo-rich column marked by yellow arrow in (c). Electron beam is parallel to $[1\bar{2}10]_{\alpha'}$ zone axis. (d) Schematic diagram showing structural model of (10$\bar{1}$1) CTB in α' lattice. Dashed purple and blue circles represent periodic atomic sites in α' martensite and its transformation twin, respectively. Letters E and C represent extension and compression sites in the CTB, respectively.

the β phase and the martensite, as marked by the yellow dashed frame 3 in Fig. 3b. The interfacial structure and OR between the β phase and the twin are identical to those between the β phase and the martensite.

Although there is a small misfit between $(101)_{\beta}$ and $(0001)_{\alpha'}$, this misfit can still cause large misfit strain over long range in the interface, which leads an array of misfit dislocation to be generated to accommodate the strain. Fig. 5a shows a large β phase formed on a (10$\bar{1}$1) CTB. It also has a Potter OR with the martensite and the twin. Careful inspection indicates that there are two misfit dislocations distributed in the β/twin interface and two misfit dislocations distributed in the β/matrix interface. The half atomic plane of one of misfit dislocations in the β/twin interface, as marked by the yellow dashed frame in Fig. 5a, is shown clearly in its corresponding inverse fast-Fourier transform (IFFT) image in Fig. 5b. The compressive and tensile strain regions caused by the misfit dislocations are shown in Fig. 5c. According to our measurements, the separation distances of misfit dislocations in the β/twin interface and β/matrix interface are 98 d(0002) and 79 d(0002), respectively. The difference of their separation distances is probably caused by the difference of local Mo concentration in the β phase, since solution of Mo in β phase can lead to a decreased lattice parameter, and the more Mo solute atoms dissolve into the β phase, the lower its lattice parameter is.

Since the Potter OR is a kind of unusual OR between the β and the α' martensite, it is necessary to investigate if it would be replaced by the Burgers OR, with the extension of the ageing time, as the Burgers OR has been frequently reported to form in titanium alloys [2,3,7]. Fig. 6 shows two larger β precipitates formed on (10$\bar{1}$1) CTBs in a sample that is aged to a later stage. The β precipitate, marked by the red arrow in Fig. 6a, has a length of ~90 nm, and its major axis is parallel to the CTBs. The length of the β precipitate, marked by the orange arrow in Fig. 6d, is approximately 120 nm, and its major axis deviates slightly from the CTBs. According to our observations, the β precipitate in Fig. 6a is still on the CTB, while the β precipitate in Fig. 6d is a retained one, around which the twin and CTB have disappeared after the long-time ageing. Even so, these two β precipitates still have the Potter OR with the martensite, as shown in Fig. 6b, c, e and f. This suggests that the Potter OR between the β and the martensite is relatively stable, and it remains during growth or coarsening of the β precipitates, even when the CTB has disappeared after a long period of ageing. Note that the β phases formed directly from the martensite and those formed at dislocation within the martensite and at the interface between two martensite plates all have the Burgers OR with the martensite, as shown in Figs. 7 and 8.

3.2. Rationlizations of Mo segregation and β precipitation

From the point of view of elastic strain minimization, the Mo segregation at compression site in {10$\bar{1}$1} CTBs seems to be expected because Mo atom (atomic radius: 0.136 nm [40]) is smaller than Ti atom (atomic radius: 0.147 nm [40]). Since it has been reported in a recent study [41] that chemical bonding can also be the major factor for the occurrence of solute segregation in CTBs, it is necessary to examine the segregation energies of Mo segregated to the compression or extension sites in the CTB to rationalize the Mo segregation phenomenon. Fig. 9a shows a supercell used to calculate segregation energies of Mo at compression or extension site in a (10$\bar{1}$1) CTB. Different Mo occupancies in a single column of extension or compression is considered in this study, as in some cases solute occupancy can significantly affect the solute segregation behavior at CTB [41]. The first-principles calculation results, Fig. 9b, show that segregation energy values are negative when Mo segregates to the compression sites, and that the minimum segregation energy is reached when the Mo occupancy in a single compressed column is 100%. These results indicate that it is energetically favored for Mo to segregate to compression sites, and that Mo tends to occupy all of the Ti sites in each of the compressed columns.

In order to understand the formation mechanism of β structure on the (10$\bar{1}$1) CTB, the relaxed structure of a (10$\bar{1}$1) CTB without Mo segregation is firstly inspected along $[1\bar{2}10]_{\alpha'}$, Fig. 10a. To examine the relationship between the (10$\bar{1}$1) CTB and the β structures, a relaxed β structural unit is shown in Fig. 10b. Note that 20 at.% Mo atoms were randomly put into the β structure during its geometrical relaxation since the Mo concentration in the β phase was measured to be approximately 20 at.%. Careful inspection reveals that the atomic arrangement surrounding the com-

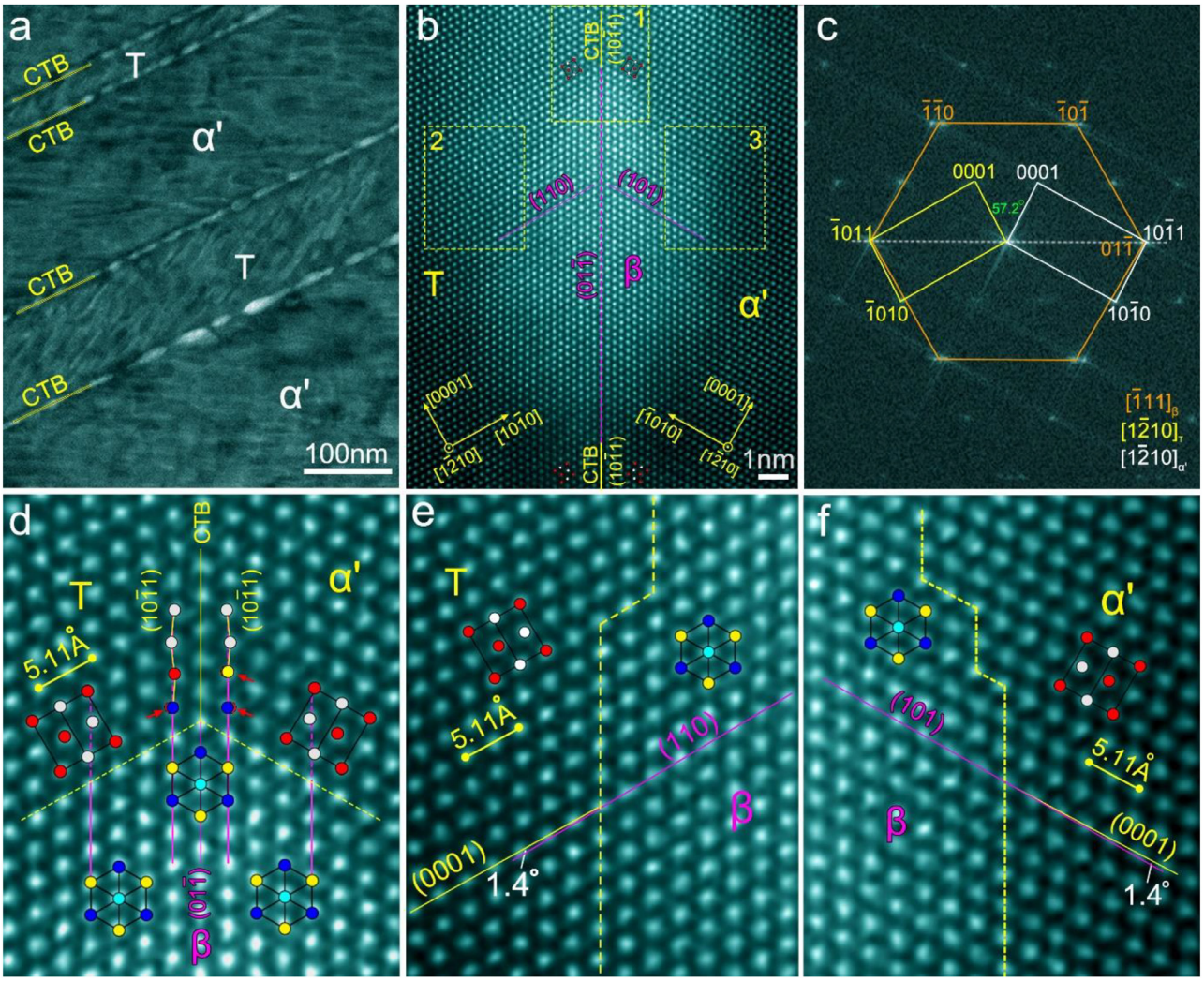

Fig. 3. (a) Low-magnification HAADF-STEM image showing β precipitates formed on (10$\bar{1}$1) CTBs in a sample aged at 550 °C for 8 h. (b) A small β phase formed on a (10$\bar{1}$1) CTB in the sample and (c) its corresponding FFT pattern. (d–f) Enlarged HAADF-STEM images of regions marked by yellow dashed frames 1 to 3 respectively in (b) showing the interfacial structures between the β phase, α' martensite and transformation twin. Red and white dots indicate positions of atomic columns in different layers in the martensite and the twin along the viewed direction, and yellow, blue and sky-blue dots indicate positions of atomic columns in β precipitate in different layers along the viewed direction. Three red arrows in (d) indicate three columns that has transformed from the martensite and twin lattices into β lattice. Yellow dashed lines in (d–f) represent interphase boundaries. Electron beam is parallel to $[1\bar{2}10]_{\alpha'}/[\bar{1}11]_\beta$.

pression site in the (10$\bar{1}$1) CTB is similar to that of the β structural unit, i.e., the surrounding six atoms of the compression site in the (10$\bar{1}$1) CTB and those of the central atom in the β structural unit are both distributed alternately in two different planes, three in the same plane and constituting a triangle, Fig. 10a and b. Thus, it is reasonable to speculate that the structure surrounding each of the compression sites in the (10$\bar{1}$1) CTB could potentially serve as a template for the formation of the β structural unit and hence induce the β precipitation if the atoms located in the compression site could be further changed to the positions of the β structure.

As Mo segregation at the compression sites occurs before β nucleation, Fig. 2, it is necessary to investigate the impact of Mo segregation on the structure of the (10$\bar{1}$1) CTB. Fig. 10c shows the relaxed structure along $[1\bar{2}10]_{\alpha'}$ where all Ti atoms in the compressed columns are substituted by Mo atoms. By comparing the surrounding structure of a compression site in the CTB without and with Mo segregation, Fig. 10a and c, it is found that the Mo segregation slightly changes the atomic bond lengths in the two triangles surrounding the compression site. For the atomic bond lengths in the triangle constituted by the orange atoms, they are changed from 4.81, 4.68 and 4.68 Å to 4.45, 4.46 and 4.46 Å, respectively. The changed bond lengths are obviously closer to that (4.54 Å) of atoms in the equilateral triangle constituted by the green atoms in the β structural unit. For the atomic bond lengths in the triangle constituted by the yellow atoms, one of the three bond lengths decreases from 4.20 to 4.13 Å, which is a little further away from the atomic bond length of 4.54 Å in the β structural unit, but the other two bond lengths are increased from 4.32 to 4.40 Å, closer to that of the edge length of the equilateral triangle. Thus, the overall change of atomic bond lengths in this triangle could also be regarded as being slightly closer to those of the triangle constituted by the sky-blue atoms in the β structural unit. Therefore, the Mo segregation at the compression sites could result in the bond lengths of its surrounding atoms in the two different planes (normal to $[1\bar{2}10]_{\alpha'}$) closer to those of atoms in the β structural unit.

To demonstrate the impact of Mo segregation on the atomic column shift within the (10$\bar{1}$1) CTB, Fig. 10d and e show the atomic arrangements within the (10$\bar{1}$1) CTB without Mo segregation and the $(01\bar{1})_\beta$ plane, respectively. As atoms within the (10$\bar{1}$1) CTB are at two different planes along [1$\bar{2}$10] and atoms within the $(01\bar{1})_\beta$ are located at three different planes along

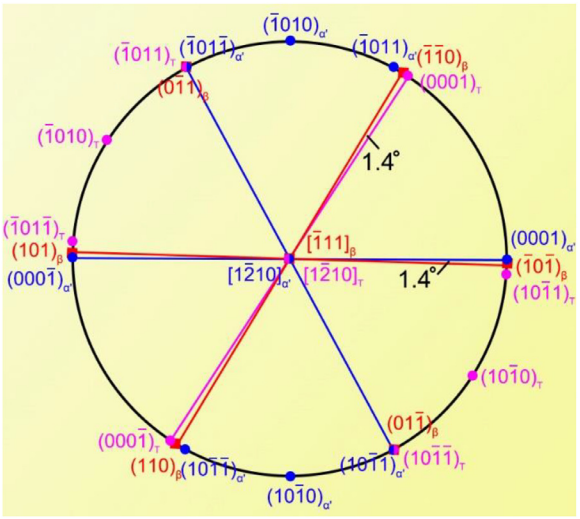

Fig. 4. Stereographic projection showing the Potter orientation relationship between β phase, α' martensite and twin. $(\bar{1}0\bar{1})_\beta$ is at 1.4° to $(0001)_{\alpha'}$ and $(\bar{1}\bar{1}0)_\beta$ is at 1.4° to $(0001)_t$.

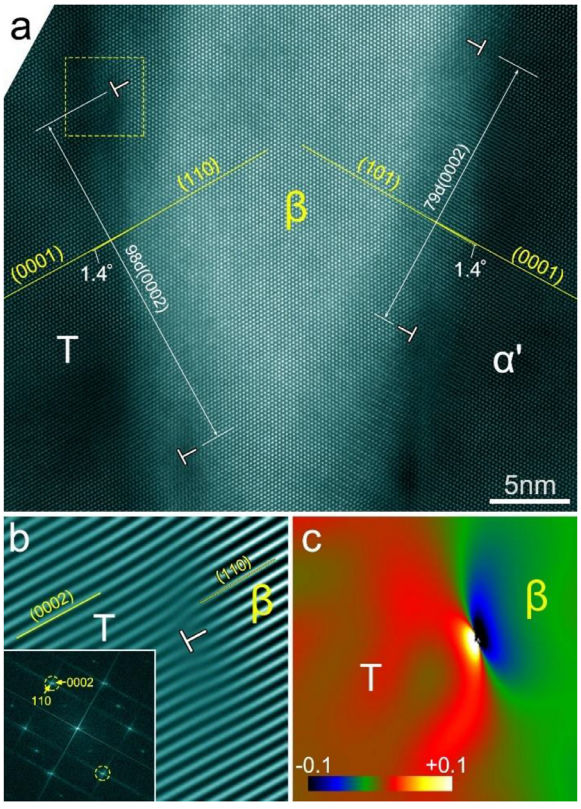

Fig. 5. (a) HAADF-STEM image showing a relatively large β phase formed on a $(10\bar{1}1)$ CTB in a sample aged at 550 °C for 8 h. (b) IFFT image of the area marked by yellow dashed frame in (a) showing a misfit dislocation in β/twin interface. Inset in (b) is the corresponding FFT pattern of the area. (c) GPA strain map calculated in the direction normal to $(0001)_t$ plane showing the compressive and tensile strain regions of the interfacial dislocation in (b). Symbol ⊥ represents a misfit dislocation. Electron beam is parallel to $[1\bar{2}10]_{\alpha'}$.

$[\bar{1}11]_\beta$, the transformation from $(10\bar{1}1)$ CTB to $(01\bar{1})_\beta$ plane inevitably involves an atomic displacement or shuffle (~0.70 Å) along $[1\bar{2}10]$ direction for atoms in compression columns in Fig. 10d. When Mo atoms segregate to the compressed columns and substitute for all Ti atoms, an out-of-plane shift of the segregated Mo atoms in each column occurs after relaxation, as indicated by the red arrows in Fig. 10f. Interestingly, this shift moves the segregated Mo atoms to almost the middle plane of its left and right atoms along $[1\bar{2}10]_{\alpha'}$ direction. As a result, the atomic shift that is needed for the formation of the $(01\bar{1})_\beta$ plane is dramatically decreased from 0.70 Å down to 0.04 Å, indicating that the Mo segregation makes the atomic arrangement on the $(10\bar{1}1)$ CTB much closer to that on the $(01\bar{1})_\beta$. Fig. 10g–j show the overlapped structures of the β structural unit and the $(10\bar{1}1)$ CTB without and with Mo segregation. While the atoms located in the six columns surrounding the compression site column (marked by letter C) are closer to the positions corresponding to the β structural unit, with the Mo segregation in the compression site column, the most striking change caused by the Mo segregation is the shift of atoms located in the compression site column to the positions almost corresponding to those of the β structural unit, as marked by the blue arrows in Fig. 10h and j. This finding further demonstrates that the occurrence of Mo segregation in the $(10\bar{1}1)$ CTB can adjust the CTB structure almost to the structure of β. Note that Mo segregation in the CTB also leads to high Mo concentration in local regions. This provides the chemical environment needed for the β precipitation. Therefore, Mo segregation is structurally and chemically beneficial for the formation of β and hence its precipitation.

To compare the difficulty of β nucleation in regions of the α' martensite away from the $(10\bar{1}1)$ CTB, first-principles calculations were made to compare the elastic strain energies caused by the formation of a β structure unit at different positions on a CTB or away from the CTB in the martensite. Fig. 11a shows a $(10\bar{1}1)$ CTB supercell with Mo segregation. Seven different positions are chosen around the CTB for the formation of β structural unit, and each position is consisted of seven atoms, one of them being at the center and surrounded by the other six atoms. To simplify the following descriptions, the central atoms of the seven different positions are marked by numbers 1 to 7, Fig. 11a, and these positions are labeled by numbers 1 to 7, respectively. Considering that the β phase formed on the $(10\bar{1}1)$ CTB has a Potter OR with α'-martensite/twin and the β phase formed within the martensite has a Burgers OR [16], the calculations of the elastic strain energy caused by the β structural unit, Fig. 11b, at different positions were made by taking the change of OR into account. When the β structural unit forms at the $(10\bar{1}1)$ CTB, i.e., positions 1 and 2, the OR is set to be the Potter OR. When the β structural unit forms within the martensite, i.e., positions 0, 5 to 7, the OR is set to be the Burgers OR. As for the positions 3 and 4, both ORs are considered because they are immediately adjacent to the CTB. Moreover, as the Mo segregation at the CTB provides a high Mo concentration, the β structural units located at positions 1 to 4 are set to include 20 at.% Mo solute, while those located at positions 0, 5 to 7 are not. According to the calculated results, Fig. 11c, the elastic strain energy caused by the β structural unit is the lowest when it forms at position 1, which suggests that the formation of the β structural unit at position 1, i.e., from the structure surrounding the compression site on the CTB, is most energetically favorable. Note that the initial structure of β at the very early stage of its formation (e.g., the saddle point configuration) may deviate from the perfect body-centered cubic (BCC) crystal lattice according to the non-classical nucleation theory. The calculated results may not quantitatively represent the real energy change induced by the formation of β structural unit, but qualitatively represent the difference of the elastic strain energies caused by the formation of a β structure unit at different positions.

4. Discussion

The present paper demonstrates the occurrence of Mo segregation in the $\{10\bar{1}1\}$ CTB in α' martensite in a Ti-4Mo alloy at the very early stage of ageing. While it is experimentally difficult to

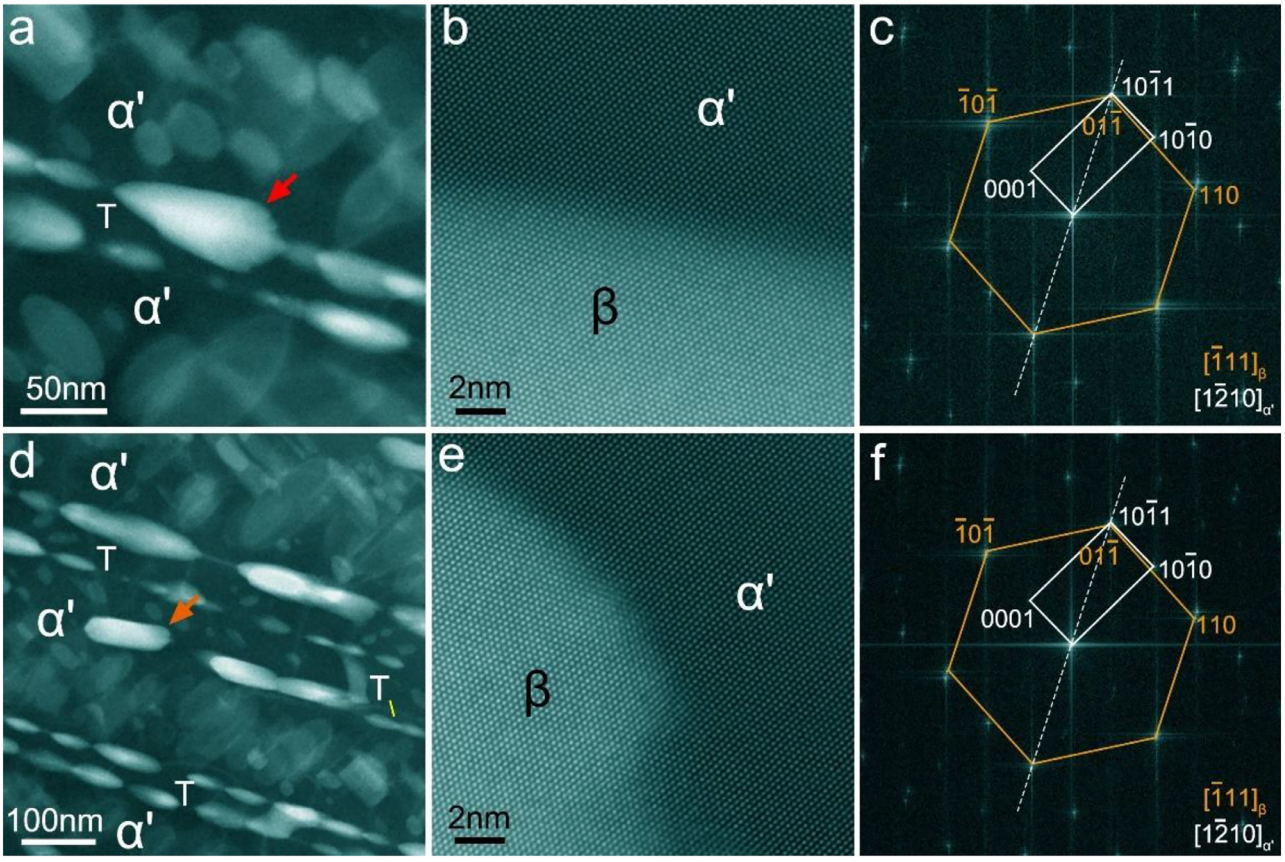

Fig. 6. (a, d) Low-magnification HAADF-STEM images showing β precipitates formed $(10\bar{1}1)$ CTBs in samples aged at 550 °C for 48 h. The β precipitate marked by the red arrow in (a) is a large one that is still on the CTB, while the β precipitate marked by the orange arrow in (d) is a retained one, around which the twin and CTB have disappeared after long-time ageing. (b, e) Atomic-resolution HAADF-STEM images and (c, f) corresponding FFT patterns showing the Potter orientation relationship between the β marked by the red arrow in (a) and the α' martensite and between the β marked by the orange arrow in (d) and the α' martensite.

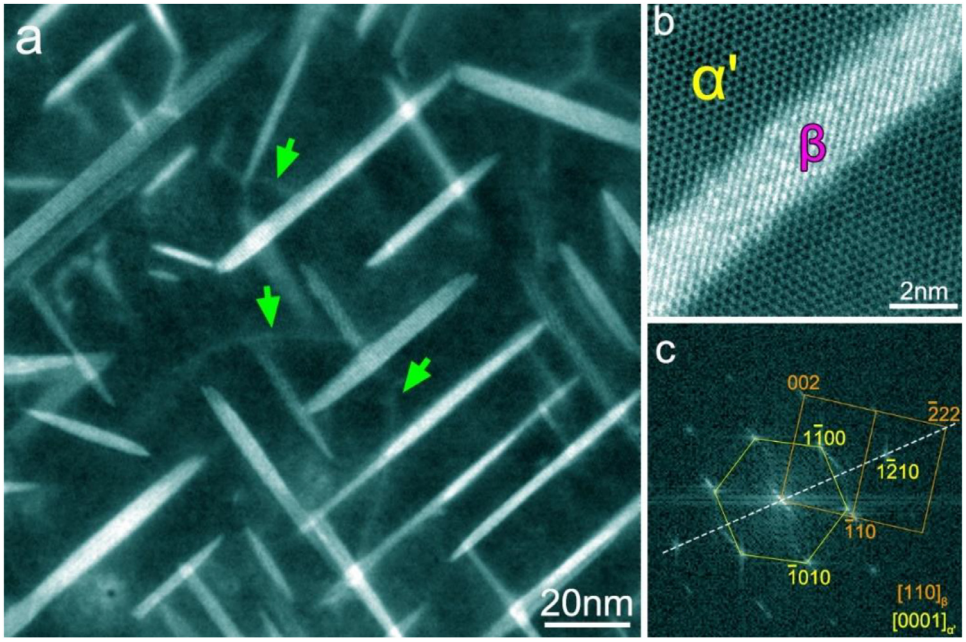

Fig. 7. (a) Low-magnification HAADF-STEM image showing β precipitates in a sample aged at 500 °C for 8 h. (b) Atomic resolution HAADF-STEM image and (c) corresponding FFT pattern of β at dislocation showing the Burgers orientation relationship between the β and α' martensite. Green arrows in (a) mark dislocations. Electron beam is parallel to $[0001]_{\alpha'}$. Note that the β precipitates formed directly from the martensite matrix is very similar to these formed at the dislocations.

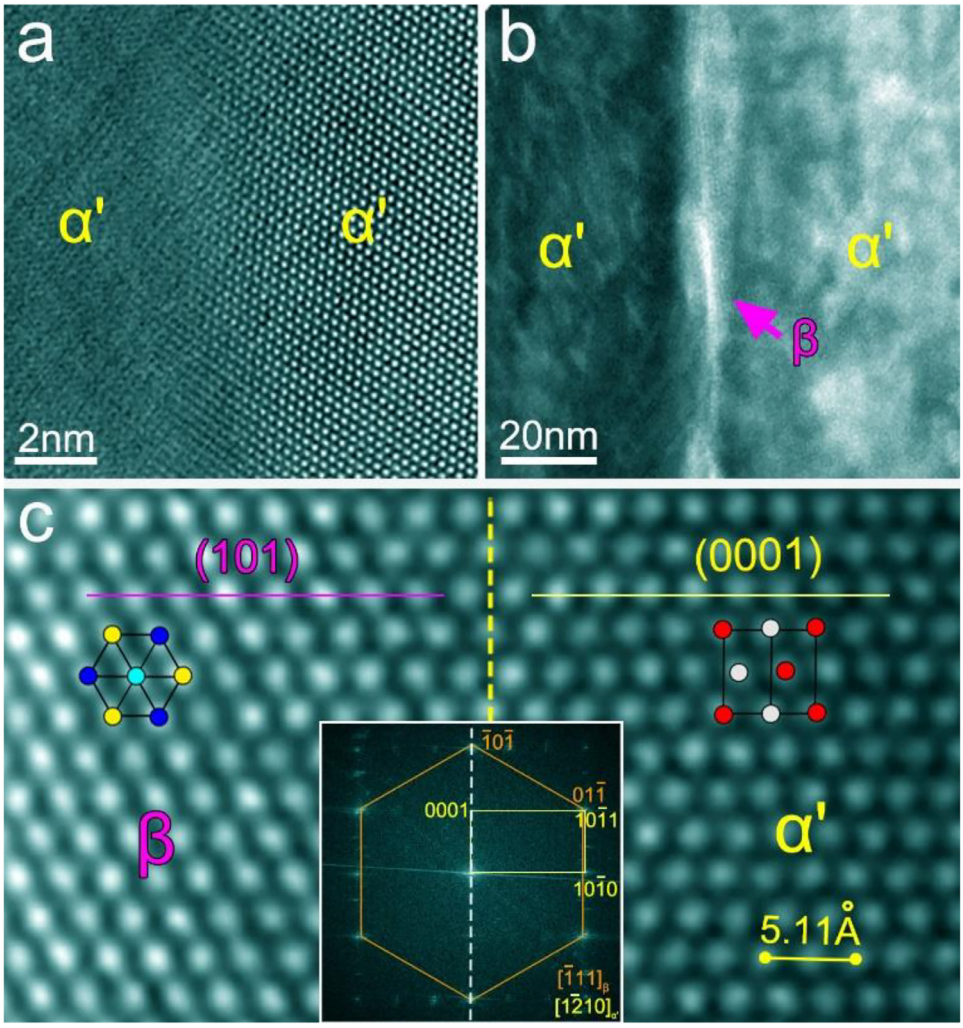

Fig. 8. HAADF-STEM images showing (a) a martensite boundary in an as-quenched sample, (b) β precipitate formed at a martensite boundary in a sample aged at 500 °C for 8 h, and (c) interfacial structure between the β in (b) and α' martensite. Inset in (c) is the corresponding FFT pattern showing the Burgers orientation relationship between the β and α' martensite. Electron beam is parallel to $[1\bar{2}10]_{\alpha'}$.

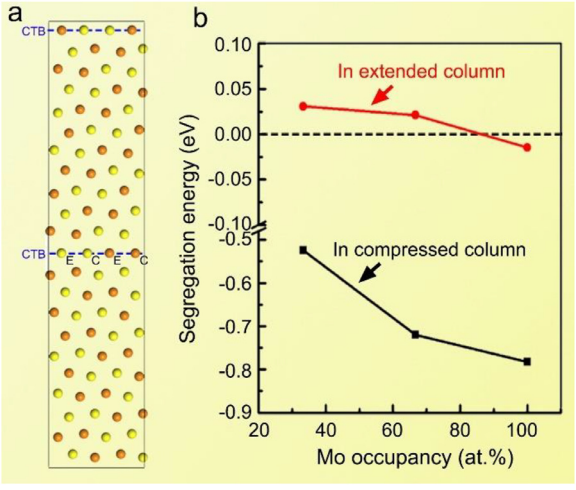

Fig. 9. (a) Supercell used to calculate segregation energies of Mo solute at compression or extension site in $(10\bar{1}1)$ CTB. Letters E and C represent extension and compression sites in the CTB, respectively. (b) First-principles calculated segregation energies of Mo with different occupancies in a single extended or compressed column in the $(10\bar{1}1)$ CTB.

quantitatively acquire the Mo concentration in the $\{10\bar{1}1\}$ CTBs because the Mo atoms are located in the single plane of the CTB, our DFT calculation results suggest that it is energetically favored for Mo to segregate to compression sites, and that Mo tends to occupy all of the compressed columns, Fig. 9b. Therefore, theoretically the maximum Mo concentration in the CTBs prior to β precipitation is 50 at.%. Mo segregation does not occur in the as-quenched sample, Fig. 1b and c, which suggests that the Mo content in the CTB in the as-quenched sample should be equal or similar to the Mo content in the alloy, i.e., 4 wt.% (~2 at.%). However, the Mo concentration in a CTB is expected to be in the range 2–50 at.% after ageing.

The Mo segregation phenomenon is similar to the periodic segregation of solute atoms in CTBs in other hexagonal structures such as magnesium alloys [41–43]. While the Mo segregation at compression site changes the bond lengths of atoms surrounding the compression atoms, Fig. 10c, a surprising change caused by the Mo segregation is an out-of-plane shift of atoms in the whole compression column, Fig. 10f. This is unusual, as solute segregation in twin boundaries in other hexagonal alloys such as magnesium [41–43] do not lead to any out-of-plane shift of solute atoms in the compression or extension column, and it may be caused by the Jahn-Teller splitting of the degenerated *d* states of Mo atom [44]. Mo segregation in the $\{10\bar{1}1\}$ CTB is not a special case in Ti alloys, the segregation of solute atoms of other alloying elements in

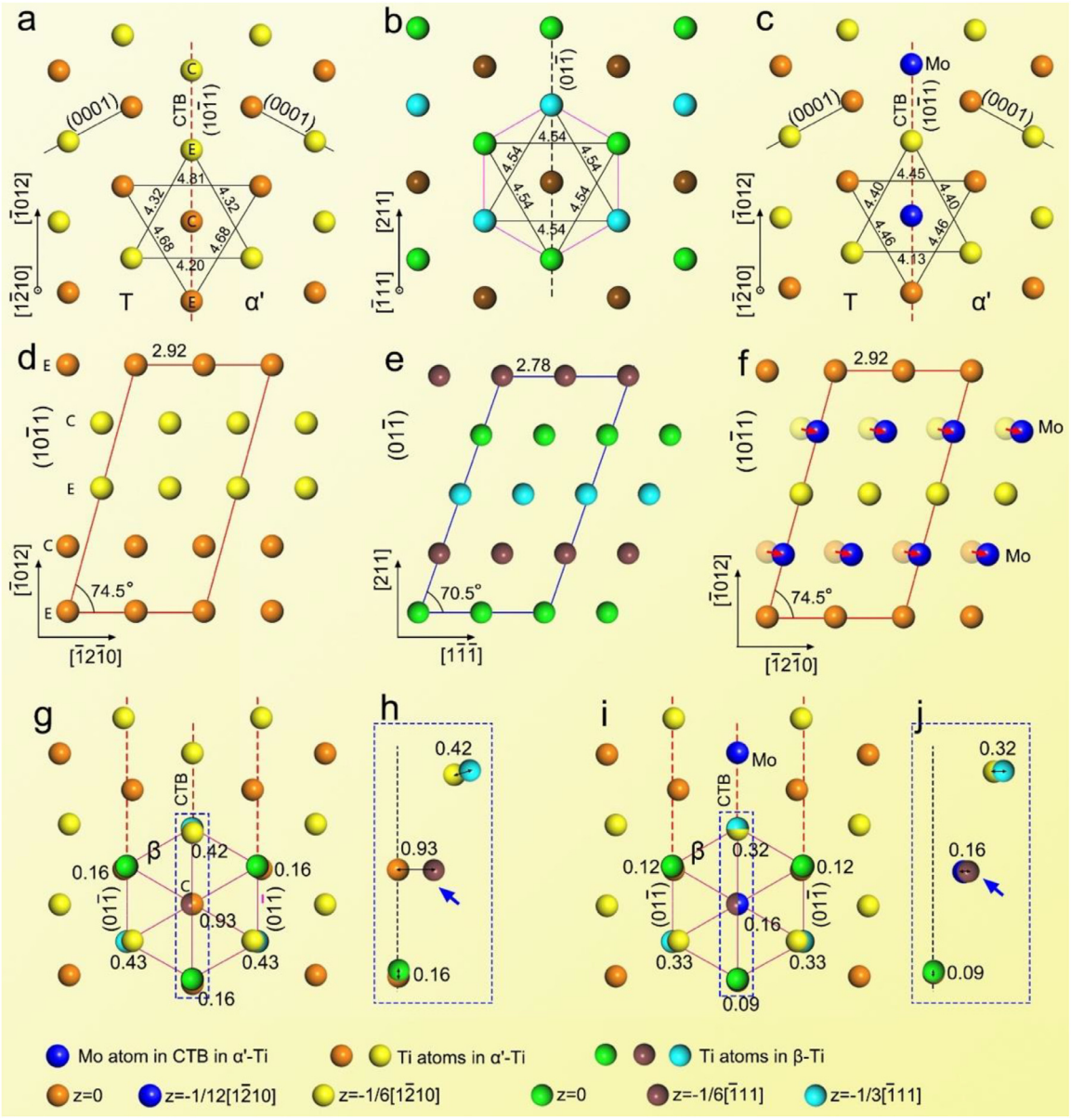

Fig. 10. (a) Relaxed structure of (10$\bar{1}$1) CTB without solute segregation. (b) Relaxed β lattice with 20 at.% Mo solute atoms distributed randomly in the β. The Mo solutes are not presented to get a clearer visualization in (b) and the pink regular hexagon marks a β structural unit. (c) Relaxed structure of (10$\bar{1}$1) CTB in which all Ti atoms at compression sites are substituted by Mo atoms. (d, e) Right side views of the CTB in (a) and (01$\bar{1}$) plane in (b), respectively. (f) Right side view of the CTB with Mo segregation in (c). Arrows in (f) represent the atomic out-of-plane shift during relaxation when Mo atoms substitute for all Ti atoms in the compression site columns. (g, i) Overlapped structures of β structural unit in (b) and CTB structures in (a) and (c), respectively. Red dashed line in (g, h) represents the extension trace of (01$\bar{1}$) plane of the β structural unit. (h, j) Right side views of the atoms in dashed blue frames in (g) and (i), respectively. Numbers in (g–j) represent the shift distances that the atoms around the compressive site should make to form a β structural unit when the green atoms in the β structural unit and the orange atoms in the CTB are on the same plane. Blue arrows in (h, j) mark the most striking change after the occurrence of Mo segregation. The units of distances between atoms are all given in Å. Miller indices consisted of three and four numbers are for β and α', respectively.

the CTB is also expected. Fig. 12 shows the segregation energies of five commonly used β stabilizing elements (V, Nb, Ta, Cr, Fe) in a {10$\bar{1}$1} CTB with 100% occupancy. All these elements have smaller atomic radius than Ti. The DFT calculation results show that V, Nb, Cr, Fe may segregate to the compression site, which is consistent with the minimization of elastic strain. Ta may segregate to the extension site, which might be due to a strong chemical bonding between the Ta solute and the surrounding Ti atoms of extension site. This resembles the unusual segregation of Bi that has a larger atomic radius than Mg to compression sites of {10$\bar{1}$1} CTB in magnesium alloys [41]. Moreover, the segregation of these solute atoms could change the atomic bond lengths surrounding the compression site in CTB as well, and in addition to Ta and Fe, the segregation of V, Nb or Cr could also lead to the occurrence of an out-of-plane shift for the segregated atoms within the CTB, as shown in Fig. 13, like Mo segregation.

It is also demonstrated in this study that heterogeneous precipitation of β phase on Mo-segregated {10$\bar{1}$1} CTBs in α' martensite occurs at the subsequent stage. This is complementary to heterogeneous precipitation of β phase on interfaces between martensite plates or on dislocations inside the martensite plates [2,16]. The precipitation of β is induced by the combined effect of the specific (10$\bar{1}$1) CTB structure in α' and Mo segregation in the CTB. The specific (10$\bar{1}$1) CTB structure is an intermediate state between

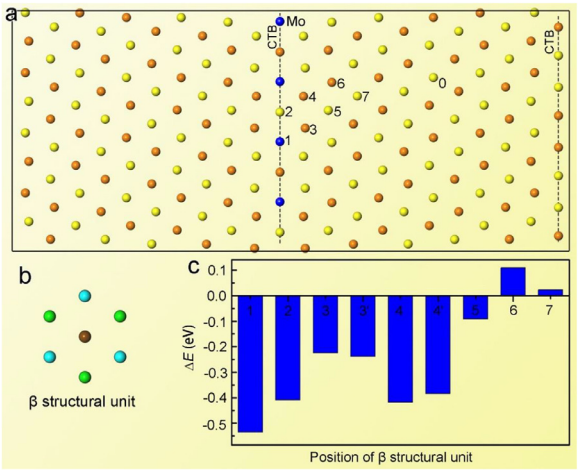

Fig. 11. (a) Supercell used for determining the energetically favored position for the formation of β structural unit. Numbers 0 and 1 to 7 represent respectively the central atoms of different positions in the α' martensite (reference state) and on/near the CTB. (b) β structural unit. Different colors in (a, b) denote atoms in different layers along (a) $[1\bar{2}10]_{\alpha'}$ and (b) $[\bar{1}11]_{\beta}$. (c) Histogram showing the difference of elastic strain energy values (ΔE) caused by β structural unit formed at positions 1 to 7 and position 0 (reference state) in (a). Positions 3 and 3′ (or 4 and 4′) represent β structural unit formed at position 3 (or 4) having Potter and Burgers ORs with α' martensite, respectively.

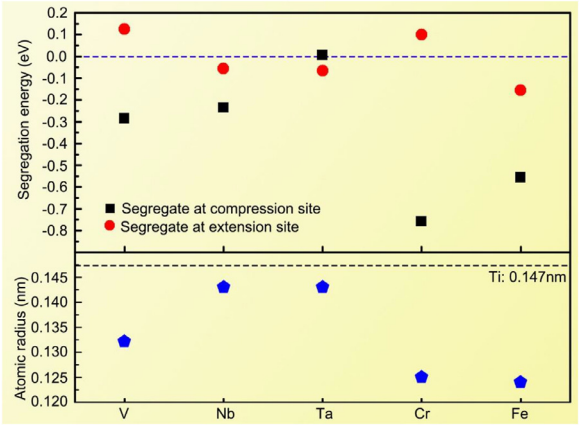

Fig. 12. Segregation energies of other commonly used β stabilizing elements at compression and extension sites in $(10\bar{1}1)$ CTB. These elements all have smaller atomic radius than Ti atom. V, Nb, Cr and Fe tend to segregate to the compression site, while Ta tends to segregate to the extension site.

the parent (α', hexagonal) and product (β, BCC) structures, Fig. 10a, which resembles that of the β phase and potentially serves as a template of the β phase embryos. After the occurrence of Mo segregation, the intermediate structure becomes almost identical to the β structure and hence hosting the β precipitation. These findings represent a major advance in the theory of heterogeneous nucleation of a precipitate phase at structure-specific twin boundaries of a parent phase and sheds light on the formation mechanism of precipitate phase in other alloy systems where deformation or annealing twins have been found to server as cradles of new product phases, such as the {332} coherent twins in BCC parent phase hosting α'' martensitic embryos and the {112} twins hosting ω phase embryos in Ti alloys [45], and {111} twins in the face-centered cubic (FCC) phase hosting γ'' (DO_{22}) phase [46] and {111} twins in $L1_2$ phase hosting embryos of χ (DO_{19}) or η (DO_{24}) embryos in Ni-base superalloys [47–49].

The β phase formed on the $(10\bar{1}1)$ CTB has a Potter OR with α', i.e., $[\bar{1}11]_{\beta}$ // $[1\bar{2}10]_{\alpha'}$ and $(01\bar{1})_{\beta}$ // $(10\bar{1}1)_{\alpha'}$, which is clearly different from the Burgers OR that has been frequently reported in the literature for β with martensite α' or equilibrium phase α [3,16,37,50,51]. The β phase with the Potter OR is more difficult to form than the β phase with the Burgers OR, since in the absence of structure-specific templates the β precipitates usually form with the Burgers OR. The presence of the $(10\bar{1}1)$ CTB provides a unique intermediate structure that is similar to that of β, which induces the formation of the Potter OR, Fig. 10. In contrast, the dislocations inside martensite, the martensite matrix and the boundaries between two plates of martensite themselves cannot provide such a unique structure-template and hence β phase with the Potter OR does not form at these places, Figs. 7 and 8. In addition, the interfacial structure and orientation relationship between β phase and martensite are identical to those between β phase and twin, Fig. 3e and f. This is due to the fact that $(10\bar{1}1)$ CTB is the mirror plane of the martensite and its twin, and $(01\bar{1})_{\beta}$ plane is the mirror plane of β structure. Since the $(10\bar{1}1)$ CTB is parallel to the $(01\bar{1})_{\beta}$ plane, the interfacial structure and orientation relationship between the β and martensite are naturally symmetrical, namely, identical to those between the β phase and the twin. This could be another reason for the formation of the Potter OR between β and martensite and its twin.

Note that $\{10\bar{1}1\}$ twins are detectable in many other $\alpha+\beta$ titanium alloys [52–55], including the workhorse alloy Ti-6Al-4V [19]. Since V, Nb and Cr atoms could also segregate to the compression site of the $\{10\bar{1}1\}$ CTB, Fig. 12, and lead to a similar out-of-plane shift for the segregated atoms within the CTB, Fig. 13, to Mo solute, the heterogenous precipitation of the β phase with an unusual Potter OR with the martensite is expected to occur in the $\alpha+\beta$ titanium alloys containing these elements. As for the $\alpha+\beta$ titanium alloys containing solely Ta or Fe, although the segregation of Ta or Fe in the $(10\bar{1}1)$ CTB may not be as important as Mo segregation in terms of promoting the formation of β structure, their segregation can provide the chemical environment for β precipitation on the CTB. Thus, the segregation of Ta or Fe may also facilitate the precipitation of β phase on the $(10\bar{1}1)$ CTB to some extent.

More generally, our findings can be extended to Ti alloys whose microstructure is dominated by α phase (having essentially the same crystal structure and lattice parameters as α' [14,26]) at room temperature and $\alpha+\beta$ at elevated temperature. If a massive amount of $\{10\bar{1}1\}$ CTBs are introduced in the α phase, which has been reported to be possible via pre-deformation [56,57], the heterogeneous precipitation of a high density of β on the $\{10\bar{1}1\}$ CTBs would occur. This offers an opportunity to control the distribution of β and then improve the mechanical properties of the alloys. According to our observations, the β precipitates formed on the CTBs are smaller than those formed elsewhere in the microstructure, which is reasonable since they have an unusual Potter OR with the α' martensite and its transformation twin and are relatively difficult to grow. This provides an interesting and powerful approach for engineering ultrafine precipitate microstructures. For example, a recent research [30] reported the possibility of forming a massive amount of nanotwins and hence twin boundaries in hexagonal Ti, which provides a template for achieving an ultrafine distribution of precipitates by invoking the mechanism we demonstrated in this study. This ultrafine distribution of precipitate is expected to make significant contribution to the alloy strength.

In addition to the $\{10\bar{1}1\}$ CTB, $\{10\bar{1}2\}$ and $\{11\bar{2}2\}$ CTBs are other types of commonly observed twin boundaries in titanium and its alloys [30,37]. The segregation energies of Mo in these two types of CTBs are also calculated in the present study using first-principles calculations. The supercells that include these two types of CTBs are shown in Figs. 14a and 15a, respectively. The segregation energy of Mo with 100% occupation at the compression or extension site in a $(10\bar{1}2)$ CTB is calculated to be −0.49 eV or −0.07 eV.

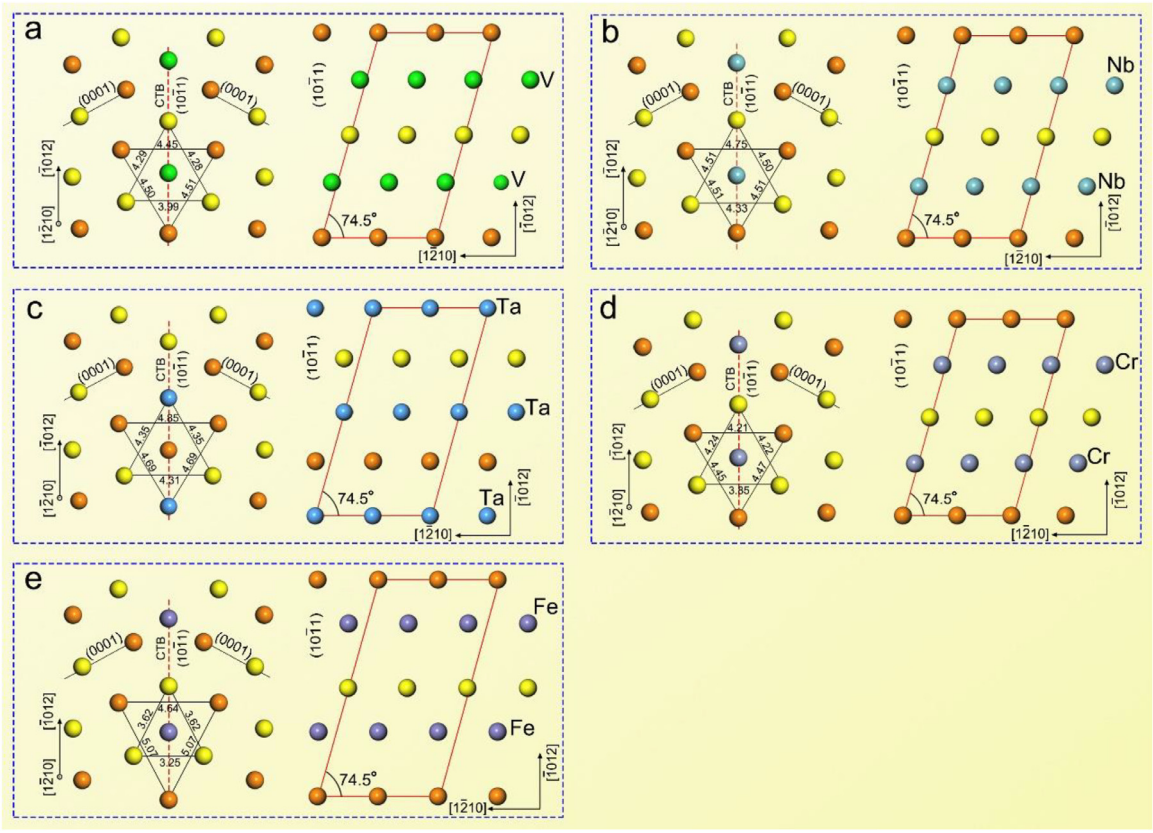

Fig. 13. Relaxed atomic structures around (10$\bar{1}$1) CTBs and corresponding atomic arrangements within the CTBs when (a) V, (b) Nb, (d) Cr, and (e) Fe segregate to compression sites and (c) Ta segregates to extension sites, respectively. Orange and yellow balls denote Ti atoms in different layers along $[1\bar{2}10]_{\alpha'}$. The units of atomic bond lengths are all given in Å.

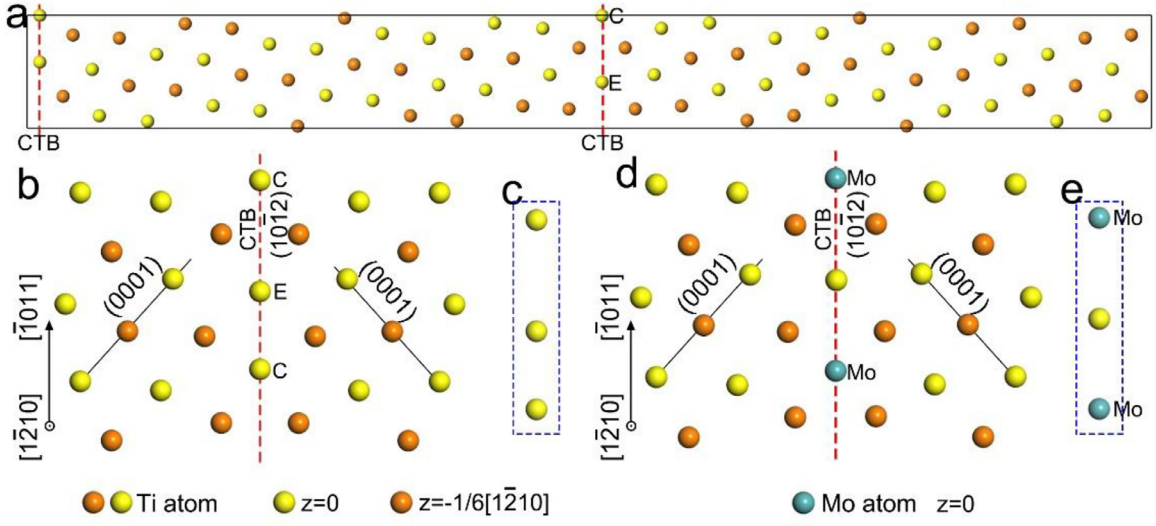

Fig. 14. (a) Supercell used to calculate segregation energy of Mo at compression or extension sites in a (10$\bar{1}$2) CTB. Letters E and C represent extension and compression sites in the CTB, respectively. (b, d) Relaxed structure of the (10$\bar{1}$2) CTB, (b) without and (d) with Mo segregation at compression sites. (c, e) Right side views of the atoms in the (10$\bar{1}$2) CTB in (b) and (d), respectively, which indicate that Mo segregation at compression sites in the (10$\bar{1}$2) CTB does not lead to an out-of-plane shift of the segregated atomic columns.

As for the {11$\bar{2}$2} CTB, there are two different types of columns within the CTB plane, similar to the {10$\bar{1}$2} CTB. However, the difference between these two columns, designated A and B in Fig. 15b, is subtle in terms of inter-atomic bond length. The segregation energy of Mo with 100% occupation at column A or B in a (11$\bar{2}$2) CTB is −0.17 eV or −0.16 eV. The value of segregation energy of Mo at the compression site in the (10$\bar{1}$2) CTB and at column A or B in the (11$\bar{2}$2) CTB are large enough to draw a strong segregation, since it has been reported that the segregation energy value of about one to several hundred meV could cause obvious solute enrichment [58]. There is currently a lack of experimental evidence in the literature to verify whether Mo segregation occurs in such CTBs. However, even if Mo segregation occurred in the (10$\bar{1}$2) and (11$\bar{2}$2) CTBs, this segregation could only provide the chemical

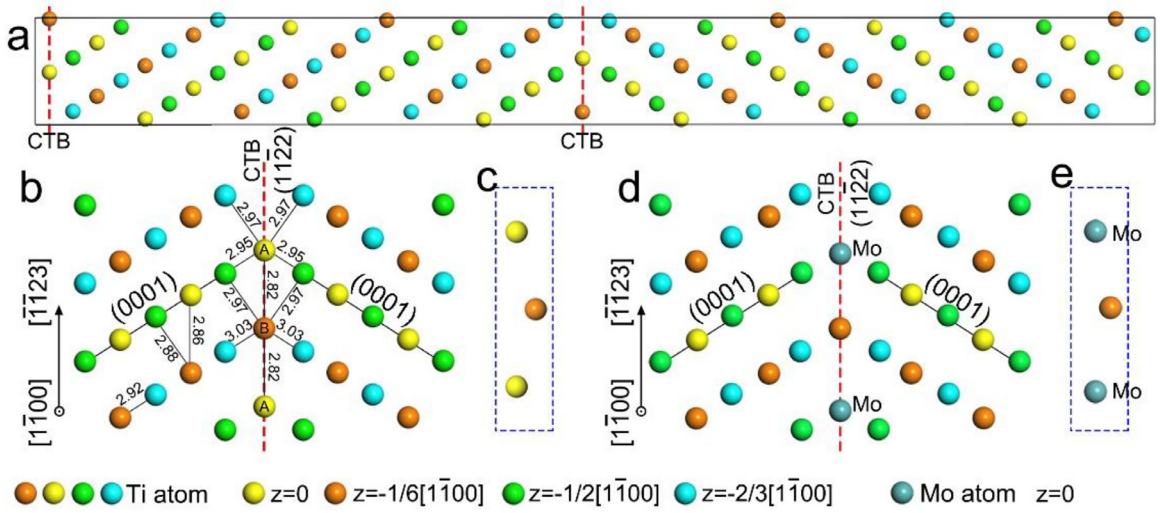

Fig. 15. (a) Supercell used to calculate segregation energy of Mo in a (11$\bar{2}$2) CTB. (b, d) Relaxed structure of the (11$\bar{2}$2) CTB, (b) without and (d) with Mo segregation in the CTB. The unit of distance between atoms in (b) is in Å. Letters A and B in (b) represent two slightly different atomic columns in the CTB. (c, e) Right side views of the atoms in the (11$\bar{2}$2) CTB in (b) and (d), respectively, which indicate that Mo segregation in the (11$\bar{2}$2) CTB does not lead to an out-of-plane shift of the segregated atomic columns.

environment for β precipitation, the structures of the (10$\bar{1}$2) and (11$\bar{2}$2) CTBs, without or with Mo segregation, are all far from that of the β phase, as shown in Figs. 14b–e and 15b–e, This distinct difference in structure makes it much less unfavorable to the formation of the β phase.

5. Conclusions

Heterogeneous precipitation of β phase on Mo-segregated {10$\bar{1}$1} CTBs within α' martensite is observed in a Ti-4wt%Mo alloy. The β precipitate formed on the CTB has a Potter orientation relationship with both martensite and its transformation twin. Its precipitation is induced by the specific structure surrounding each of the compression sites in the CTB and the Mo segregation in the CTB. The specific structure is an intermediate state between the hexagonal α' parent and the BCC β product, hence potentially serves as a host of the β phase embryos. The Mo segregation in the CTB leads to an unusual out-of-plane shift of the segregated atomic columns, which not only makes the intermediate structure almost identical to that of the β phase, but also provides a high Mo concentration needed for β phase precipitation. First-principles calculations results suggest that formation of β on the CTB with Mo segregation is energetically favorable. These findings are potentially applicable to a group of titanium alloys and even other metallic alloys such as those based on zirconium, and they not only advance the theory of heterogenous nucleation of precipitate on specific boundary structures, but also provide a novel twin-boundary-based approach to rationally design ultrafine precipitate microstructures to achieve potentially unprecedented mechanical properties.

Declaration of Competing Interest

The authors declare that they have no known competing financial interests or personal relationships that could have appeared to influence the work reported in this paper.

Acknowledgments

The study is financially supported by the Science and Technology Innovation Program of Hunan Province (No. 2022RC3035), National Natural Science Foundation of China (No. 52101167), Natural Science Foundation of Hunan Province (2022JJ40604) and State Key Laboratory of Powder Metallurgy. YW acknowledges the support from the US National Science Foundation under Grant DMR-1923929, which has facilitated this international collaboration. JFN is grateful to the support from the Australian Research Council (DP200102985 and DP190102373) and the computational resources provided by the Australian Government through NCI-Gadi and Pawsey-Magnus under the National Computational Merit Allocation Scheme. This work was supported in part by the High Performance Computing Center of Central South University and Double Cs-corrected TEM Laboratory of the State Key Laboratory of Powder Metallurgy.

References

[1] D. Banerjee, J.C. Williams, Perspectives on titanium science and technology, Acta Mater. 61 (2013) 844–879.
[2] G. Lutjering, J.C. Williams, Titanium, 2nd ed., Springer, Berlin, 2007.
[3] I. Polmear, D. StJohn, J.F. Nie, M. Qian, Light Alloys, 5th ed., Elsevier, Boston, 2017.
[4] W. Xu, M. Brandt, S. Sun, J. Elambasseril, Q. Liu, K. Latham, K. Xia, M. Qian, Additive manufacturing of strong and ductile Ti–6Al–4V by selective laser melting via *in situ* martensite decomposition, Acta Mater. 85 (2015) 74–84.
[5] M. Simonelli, Y. Tse, C. Tuck, The formation of $\alpha+\beta$ microstructure in as-fabricated selective laser melting of Ti–6Al–4V, J. Mater. Res. 29 (2014) 2028–2035.
[6] L. Kang, C. Yang, A review on high-strength titanium alloys: microstructure, strengthening, and properties, Adv. Eng. Mater. 21 (2019) 1801359.
[7] S.A. Mantri, D. Choudhuri, T. Alam, G.B. Viswanathan, J.M. Sosa, H.L. Fraser, R. Banerjee, Tuning the scale of α precipitates in β-titanium alloys for achieving high strength, Scr. Mater. 154 (2018) 139–144.
[8] Z. Du, Y. Ma, F. Liu, X. Zhao, Y. Chen, G. Li, G. Liu, Y. Chen, Improving mechanical properties of near beta titanium alloy by high-low duplex aging, Mater. Sci. Eng. A 754 (2019) 702–707.
[9] R. Guo, B. Liu, R. Xu, Y. Cao, J. Qiu, F. Chen, Z. Yan, Y. Liu, Microstructure and mechanical properties of powder metallurgy high temperature titanium alloy with high Si content, Mater. Sci. Eng. A 777 (2020) 138993.
[10] S.L. Semiatin, T.R. Bieler, The effect of alpha platelet thickness on plastic flow during hot working of TI–6Al–4V with a transformed microstructure, Acta Mater. 49 (2001) 3565–3573.
[11] P.F. Ji, B. Li, S.G. Liu, X. Zhang, B.H. Chen, X.Y. Zhang, M.Z. Ma, R.P. Liu, Controlling the corrosion behavior of Ti-Zr alloy by tuning the α/β phase volume fraction and morphology of β phase, J. Alloy. Compd. 825 (2020) 154153.
[12] Z. Zhao, J. Chen, H. Tan, G. Zhang, X. Lin, W. Huang, Achieving superior ductility for laser solid formed extra low interstitial Ti-6Al-4V titanium alloy through equiaxial alpha microstructure, Scr. Mater. 146 (2018) 187–191.
[13] J. Sieniawski, W. Ziaja, K. Kubiak, M. Motyka, Microstructure and mechanical properties of high strength two-phase titanium alloys, Titanium Alloys-Advances in Properties Control, InTech, Rijeka, 2013.
[14] L. Thijs, F. Verhaeghe, T. Craeghs, J.V. Humbeeck, J.P. Kruth, A study of the microstructural evolution during selective laser melting of Ti–6Al–4V, Acta Mater. 58 (2010) 3303–3312.
[15] R. Davis, H.M. Flower, D.R.F. West, Martensitic transformations in Ti-Mo alloys, J. Mater. Sci. 14 (1979) 712–722.

[16] R. Davis, H.M. Flower, D.R.F. West, The decomposition of Ti-Mo alloy martensites by nucleation and growth and spinodal mechanisms, Acta Metall. 27 (1979) 1041–1052.
[17] S.Q. Wu, Y.J. Lu, Y.L. Gan, T.T. Huang, C.Q. Zhao, J.J. Lin, S. Guo, J.X. Lin, Microstructural evolution and microhardness of a selective-laser-melted Ti–6Al–4V alloy after post heat treatments, J. Alloy. Compd. 672 (2016) 643–652.
[18] K. Sato, H. Matsumoto, A. Chiba, T.J. Konno, Aging effect on microstructure of cold groove-rolled α'-type Ti-12 mass%V-2 mass%Al alloys studied by transmission electron microscopy, Mater. Trans. 55 (2014) 763–767.
[19] S. Cao, R. Chu, X. Zhou, K. Yang, Q. Jia, C.V.S. Lim, A. Huang, X. Wu, Role of martensite decomposition in tensile properties of selective laser melted Ti-6Al-4V, J. Alloy. Compd. 744 (2018) 357–363.
[20] E. Sallica-Leva, R. Caram, A.L. Jardini, J.B. Fogagnolo, Ductility improvement due to martensite α' decomposition in porous Ti–6Al–4V parts produced by selective laser melting for orthopedic implants, J. Mech. Behav. Biomed. Mater. 54 (2016) 149–158.
[21] J. Haubrich, J. Gussone, P. Barriobero-Vila, P. Kürnsteiner, E.A. Jägle, D. Raabe, N. Schell, G. Requena, The role of lattice defects, element partitioning and intrinsic heat effects on the microstructure in selective laser melted Ti-6Al-4V, Acta Mater. 167 (2019) 136–148.
[22] K. Sato, H. Matsumoto, K. Kodaira, T.J. Konno, A. Chiba, Phase transformation and age-hardening of hexagonal α' martensite in Ti–12mass%V–2mass%Al alloys studied by transmission electron microscopy, J. Alloy. Compd. 506 (2010) 607–614.
[23] H. Yu, W. Li, S. Li, H. Zou, T. Zhai, L. Liu, Study on transformation mechanism and kinetics of α' martensite in TC4 alloy isothermal aging process, Crystals 10 (2020) 229.
[24] J. Li, H.M. Wang, Aging response of laser melting deposited Ti–6Al–2Zr–1Mo–1V alloy, Mater. Sci. Eng. A 560 (2013) 193–199.
[25] X. Tan, Y. Kok, W.Q. Toh, Y.J. Tan, M. Descoins, D. Mangelinck, S.B. Tor, K.F. Leong, C.K. Chua, Revealing martensitic transformation and α/β interface evolution in electron beam melting three-dimensional-printed Ti-6Al-4V, Sci. Rep. 6 (2016) 26039.
[26] P. Villars, L.D. Calvert, Pearson's Handbook of Crystallographic Data for Intermetallic Phases, American Society for Metals Metals Park, OH, 1985.
[27] X. Fu, X.D. Wang, B. Zhao, Q. Zhang, S. Sun, J.J. Wang, W. Zhang, L. Gu, Y. Zhang, W.Z. Zhang, W. Wen, Z. Zhang, L.Q. Chen, Q. Yu, E. Ma, Atomic-scale observation of non-classical nucleation-mediated phase transformation in a titanium alloy, Nat. Mater. 21 (2022) 290–296.
[28] H. Wang, Q. Chao, H.S. Chen, Z.B. Chen, S. Primig, W. Xu, S.P. Ringer, X.Z. Liao, Formation of a transition V-rich structure during the α' to $\alpha+\beta$ phase transformation process in additively manufactured Ti-6Al-4V, Acta Mater. 235 (2022) 118104.
[29] C. Yan, Y. Xin, X.B. Chen, D. Xu, P.K. Chu, C. Liu, B. Guan, X. Huang, Q. Liu, Evading strength-corrosion tradeoff in Mg alloys via dense ultrafine twins, Nat. Commun. 12 (2021) 4616.
[30] S. Zhao, R. Zhang, Q. Yu, J. Ell, O.R. Robert, M.M. Andrew, Cryoforged nanotwinned titanium with ultrahigh strength and ductility, Science 373 (2021) 1363–1368.
[31] G. Kresse, J. Furthmüller, Efficient iterative schemes for ab initio total-energy calculations using a plane-wave basis set, Phys. Rev. B 54 (1996) 11169–11186.
[32] J.P. Perdew, K. Burke, M. Emzerhof, Generalized gradient approximation made simple, Phys. Rev. Lett. 77 (1996) 3865–3868.
[33] G. Kresse, D. Joubert, From ultrasoft pseudopotentials to the projector augmented-wave method, Phys. Rev. B 59 (1999) 1758–1775.
[34] P.E. Blöchl, Projector augmented-wave method, Phys. Rev. B 50 (1994) 17953–17979.
[35] J.D. Pack, H.J. Monkhorst, Special points for Brillouin-zone integrations"-a reply, Phys. Rev. B 16 (1977) 1748–1749.
[36] M. Motyka, Martensite formation and decomposition during traditional and AM processing of two-phase titanium alloys—an overview, Metals 11 (2021) 481 (Basel).
[37] Z. Tarzimoghadam, S. Sandlöbes, K.G. Pradeep, D. Raabe, Microstructure design and mechanical properties in a near-α Ti–4Mo alloy, Acta Mater. 97 (2015) 291–304.
[38] Q. Sun, X.Y. Zhang, Y. Ren, J. Tu, Q. Liu, Interfacial structure of $\{10\bar{1}2\}$ twin tip in deformed magnesium alloy, Scr. Mater. 90-91 (2014) 41–44.
[39] J. Tu, X.Y. Zhang, J. Wang, Q. Sun, Q. Liu, Structural characterization of {102} twin boundaries in cobalt, Appl. Phys. Lett. 103 (2013) 103.
[40] A. Takeuchi, A. Inoue, Classification of bulk metallic glasses by atomic size difference, heat of mixing and period of constituent elements and its application to characterization of the main alloying element, Mater. Trans. 46 (2005) 2817–2829.
[41] C. He, Z. Li, H. Chen, N. Wilson, J.F. Nie, Unusual solute segregation phenomenon in coherent twin boundaries, Nat. Commun. 12 (2021) 722.
[42] X. Zhao, H. Chen, N. Wilson, Q. Liu, J.F. Nie, Direct observation and impact of co-segregated atoms in magnesium having multiple alloying elements, Nat. Commun. 10 (2019) 3243.
[43] J. Nie, Y. Zhu, J. Liu, X. Fang, Periodic segregation of solute atoms in fully coherent twin boundaries, Science 340 (2013) 957–960.
[44] Q.M. Hu, R. Yang, Unconventional non-uniform local lattice distortion in dilute Ti-Mo solid solution, Acta Mater. 197 (2020) 91–96.
[45] Q. Liang, Z. Kloenne, Y. Zheng, D. Wang, S. Antonov, Y. Gao, Y. Hao, R. Yang, Y. Wang, H.L. Fraser, The role of nano-scaled structural non-uniformities on deformation twinning and stress-induced transformation in a cold rolled multifunctional β-titanium alloy, Scr. Mater. 177 (2020) 181–185.
[46] Z. Zhang, Z. Yang, S. Lu, A. Harte, R. Morana, M. Preuss, Strain localisation and failure at twin-boundary complexions in nickel-based superalloys, Nat. Commun. 11 (2020) 4890.
[47] T.M. Smith, B.S. Good, T.P. Gabb, B.D. Esser, A.J. Egan, L.J. Evans, D.W. McComb, M.J. Mills, Effect of stacking fault segregation and local phase transformations on creep strength in Ni-base superalloys, Acta Mater. 172 (2019) 55–65.
[48] T.M. Smith, B.D. Esser, N. Antolin, A. Carlsson, R.E.A. Williams, A. Wessman, T. Hanlon, H.L. Fraser, W. Windl, D.W. McComb, M.J. Mills, Phase transformation strengthening of high-temperature superalloys, Nat. Commun. 7 (2016) 13434.
[49] A.J. Egan, Y. Rao, G.B. Viswanathan, T.M. Smith, M. Mills, Effect of Nb alloying addition on local phase transformation at microtwin boundaries in nickel-based superalloys, Superalloys, Springer, Berlin, 2020, p. 2020.
[50] J.F. Nie, Orientation relationship, shape change and their traces in electron diffraction patterns and high-resolution transmission electron microscopy images, Acta Mater. 56 (2008) 3169–3176.
[51] M.X. Zhang, P.M. Kelly, Crystallographic features of phase transformations in solids, Prog. Mater. Sci. 54 (2009) 1101–1170.
[52] H. Matsumoto, S. Watanabe, S. Hanada, α' Martensite Ti–V–Sn alloys with low Young's modulus and high strength, Mater. Sci. Eng. A 448 (2007) 39–48.
[53] S. Guo, Q. Meng, X. Cheng, X. Zhao, α' Martensite Ti–10Nb–2Mo–4Sn alloy with ultralow elastic modulus and high strength, Mater. Lett. 133 (2014) 236–239.
[54] W. Ma, S. Liu, X. Zhang, B. Chen, F. Wang, X. Zhang, M. Ma, R. Liu, Microstructural evolution and mechanical properties of hot-rolled Ti-30Zr-5Al-2.5Sn alloy with mixed α and α' phases, Mater. Sci. Eng. A 792 (2020) 139812.
[55] D. Qiu, M. Zhang, P. Kelly, T. Furuhara, Discovery of plate-shaped athermal ω phase forming pairs with α' martensite in a Ti–5.26 wt.% Cr Alloy, Scr. Mater. 69 (2013) 752–755.
[56] H. Matsumoto, H. Yoneda, D. Fabregue, E. Maire, A. Chiba, F. Gejima, Mechanical behaviors of Ti–V–(Al, Sn) alloys with α' martensite microstructure, J. Alloy. Compd. 509 (2011) 2684–2692.
[57] N.E. Paton, W.A. Backofen, Plastic deformation of titanium at elevated temperatures, Metall. Trans. 1 (1970) 2839–2847.
[58] L. Feng, Y. Rao, M. Ghazisaeidi, M.J. Mills, Y. Wang, Quantitative prediction of Suzuki segregation at stacking faults of the γ' phase in Ni-base superalloys, Acta Mater. 200 (2020) 223–235.